Noname manuscript No.
(will be inserted by the editor)

Reconstruction of Sparse Recurrent Connectivity and Inputs from the Nonlinear Dynamics of Neuronal Networks

Victor J. Barranca

Received: date / Accepted: date

Abstract Reconstructing the *recurrent* structural connectivity of neuronal networks is a challenge crucial to address in characterizing neuronal computations. While directly measuring the detailed connectivity structure is generally prohibitive for large networks, we develop a novel framework for reverse-engineering large-scale recurrent network connectivity matrices from neuronal dynamics by utilizing the widespread sparsity of neuronal connections. We derive a linear input-output mapping that underlies the irregular dynamics of a model network composed of both excitatory and inhibitory integrate-and-fire neurons with pulse coupling, thereby relating network inputs to evoked neuronal activity. Using this embedded mapping and experimentally feasible measurements of the firing rate as well as voltage dynamics in response to a relatively small ensemble of random input stimuli, we efficiently reconstruct the recurrent network connectivity via compressive sensing techniques. Through analogous analysis, we then recover high dimensional natural stimuli from evoked neuronal network dynamics over a short time horizon. This work provides a generalizable methodology for rapidly recovering sparse neuronal network data and underlines the natural role of sparsity in facilitating the efficient encoding of network data in neuronal dynamics.

Keywords Network Reconstruction · Nonlinear Dynamics · Mean-Field Analysis · Signal Processing · Integrate-And-Fire Model Networks

Victor J. Barranca
Swarthmore College, 500 College Avenue, Swarthmore, PA, 19081, USA
Tel.: +1-610-328-8560
E-mail: vbarran1@swarthmore.edu

1 Introduction

Obtaining accurate and simultaneous measurements of both the detailed structure and activity of large-scale neuronal networks remains a missing yet critical component in more completely characterizing cognitive processes. While modern technological advances have made it possible to record the dynamics of increasingly large numbers of neurons, through, for example, multielectrode arrays (Field et al. 2010; Shimono and Beggs 2015; Boulton et al. 1990), genetically encoded indicators (Xu et al. 2017), and calcium imaging (Grewe et al. 2010), the reconstruction of structural neuronal connectivity is still limited to relatively small networks.

The scale and fidelity of neuronal connectivity measurements have improved in recent years; however, even with each novel experimental methodology, numerous difficulties remain in recovering the complex topology of large neuronal networks. While tracer injections can discern the fine-resolution structural connections between neurons, their application thus far has been primarily restricted to relatively small networks (Markov et al. 2013; Wall et al. 2010; Briggman and Bock 2012). As a whole, numerous limitations, such as those arising from the spatial resolution of measurement devices (Stevenson et al. 2008), synaptic diversity (Sawatari and Callaway 2000), hidden neurons (de Abril et al. 2018; Horwitz 2003), and short-time synaptic plasticity (Boccaletti et al. 2006; Song et al. 2005), still prove to be additional difficult hurdles to overcome in directly measuring the detailed connectivity of large neuronal networks. Recent studies have successfully recovered the detailed anatomical connectivity for networks of thousands of neurons in the cerebral cortex using cutting-edge approaches (Jiang et al. 2015), but there

remains a long road forward in characterizing the complete neuronal connection structure for most organisms.

In this work, we formulate a novel methodology for reconstructing the recurrent connectivity of model neuronal networks with spiking dynamics by taking advantage of their sparse network structure and intrinsic linear input-output mappings. Our method utilizes short-time measurements of the neuronal firing dynamics and voltage traces in response to an ensemble of random input stimuli. While we apply our methodology to the dynamics generated from a model network, the developed framework is potentially generalizable to experimental settings through intracellular or multielectrode array recordings in response to optogenetic forcing (Rickgauer et al. 2014; Packer et al. 2015). Results may be validated in experimental settings using the measured strengths of recurrent connections in a smaller subset of the network, which are typically estimated based on the number of synaptic contacts and postsynaptic density area observed via electron microscope or based on measured postsynaptic potential amplitudes (Barros-Zulaica et al. 2019; Holler et al. 2021).

Several alternative mathematical and statistical techniques have furnished improvements in recovering network structure from measurements of neuronal activity, including Granger causality analysis (Zhou et al. 2013), partial spectral coherence (Dahlhaus et al. 1997), maximum likelihood estimation (Zaytsev et al. 2015), phase response properties (Cestnik and Rosenblum 2017), and transfer entropy (Vicente et al. 2011; Stetter et al. 2012). Each previous method, however, has restrictions preventing practical use in effectively recovering large-scale network connectivity, such as requiring prohibitively large neuronal activity data sets (Zhou et al. 2013; Zaytsev et al. 2015; Stetter et al. 2012), addressing only excitatory network connections (Cestnik and Rosenblum 2017; Vicente et al. 2011), or failing to appropriately reconcile nonlinear dynamics in the vicinity of action potentials (Dahlhaus et al. 1997). Our theoretical framework addresses each of these issues. It is increasingly efficient for larger networks, requires short-time measurements, takes into account nonlinear activity, and reconstructs connections among both excitatory as well as inhibitory neurons.

Considering the connectivity among individual neurons is generally *sparse*, as indicated from experimental measurements in diverse brain regions (Markram et al. 1997; Ganmor et al. 2011; He et al. 2007), our methodology makes specific use of the sparse connectivity structure via compressive sensing (CS) theory (Candes et al. 2006; Donoho 2006), yielding accurate reconstructions of network data with limited measurements of neuronal dynamics. While prior methods utilized sparse structure to reconstruct *feed-forward* connectivity in pulse-coupled networks (Barranca et al. 2016b), this work overcomes the previously unaddressed difficulties in recovering *recurrent* network connectivity, which is in general significantly more difficult. Since recurrent connectivity information may be obscured by feed-forward inputs and because higher-order functional correlations in neuronal activity do not necessarily imply a true structural recurrent connection between neurons due to, for example, the influence of indirect connections (Salinas and Sejnowski 2001; Tsodyks and Gilbert 2004; Friston 2011), an alternative approach is necessary to well characterize recurrent network structure.

Through direct comparison with the known recurrent connectivity matrix generated in silico, we are able to validate the accuracy of our reconstructions. Based on the small incurred errors, we view the reconstructed recurrent connectivity matrix for the neuronal network of interest as an estimate of the true structural recurrent connectivity, which is known to be correlated with but generally distinct from the more easily inferred functional recurrent connectivity (Hagmann et al. 2008; Honey et al. 2009). We note that there are several limitations involved in applying this methodology in experimental settings, as considered in detail in the Discussion, but nonetheless we lay the theoretical groundwork for further advances in efficient structural connectivity reconstructions that may leverage sparsity and linear network response properties in the asynchronous dynamical regime. Beyond reconstructing recurrent network interactions, our framework demonstrates that high dimensional and detailed input stimuli may be similarly recovered from the evoked network dynamics by making efficient use of the typical sparse structure of natural stimuli (Field et al. 2010), imparting further insights into the efficient encoding of network data through neuronal dynamics.

The study is organized as follows. In Section 2.1, we formulate the pulse-coupled balanced network model with detailed voltage dynamics to be used in our analysis and in Section 2.2 we then derive the underlying linear map between the input stimuli and neuronal network response pivotal in relating the network structure and function. In Section 3.1, we develop our theoretical framework for reconstructing the recurrent network connectivity and, in Section 3.2, we further analyze the efficiency of our methodology with respect to the time over which network dynamics are recorded and the input ensemble size utilized. We demonstrate in Section 3.3 how our analysis naturally generalizes to recovering detailed network inputs and finally examine potential extensions as well as implications of our work in Section 4.

2 Model and Methods

2.1 Network Model

The network model we consider is composed of N neurons, such that N_E are excitatory and N_I are inhibitory, with each governed by pulse-coupled integrate-and-fire (I&F) neuronal dynamics. The I&F model has been shown to well reproduce both subthreshold membrane potential dynamics as well as firing statistics measured in experiment and has been utilized in a host of theoretical investigations of brain network computations (Mather et al. 2009; Rauch et al. 2003; Barranca et al. 2014a; Rangan and Cai 2006; Burkitt 2006; Abbott 1999; van Vreeswijk and Sompolinsky 1996). In formulating the network structure and resultant dynamical regime, we utilize balanced network connectivity (van Vreeswijk and Sompolinsky 1996; 1998; Troyer and Miller 1997; Miura et al. 2007; Barranca et al. 2019b; Barranca and Zhou 2019), yielding irregular and asynchronous dynamics important in our subsequent derivation of the network input-output mapping.

The membrane-potential (voltage) of the i^{th} neuron in k^{th} population of the I&F network, v_k^i, has activity dictated by dynamical system (subscripts $k = E$ and $k = I$ denote excitatory and inhibitory neurons, respectively)

$$\frac{dv_k^i}{dt} = -g_L(v_k^i - V_k^{Re}) + \sum_{\substack{j=1\\ j\neq i}}^{N_E} R_{kE}^{ij} \sum_l \delta(t - \tau_E^{jl}) + \sum_{\substack{j=1\\ j\neq i}}^{N_I} R_{kI}^{ij} \sum_l \delta(t - \tau_I^{jl}) + \sum_j F_k^{ij} p_k^j, \tag{1}$$

evolving from reset potential, V_k^{Re}, until arriving at the threshold potential, V_k^T, at which time the neuron is said to spike (or fire an action potential). Once a neuron spikes, its membrane potential v_k^i is instantaneously reset to the value V_k^{Re} and the membrane potential of all post-connected neurons is offset as a result of integrating over the Dirac delta functions $\delta(\cdot)$ in Eq. (1). Such spike times for the i^{th} neuron in the k^{th} population are denoted τ_k^{il} and indexed by $l = 1, 2, \ldots$ in ordering the spiking events. In simulation, the membrane potential is nondimensionalized such that $V_k^{Re} = 0$ and $V_k^T = 1$, with $g_L = 50\text{s}^{-1}$ corresponding to a typical membrane-potential time-scale of 20ms (McLaughlin et al. 2000; Barranca et al. 2014b; Brette et al. 2007).

The $N \times N$ recurrent connectivity matrix, $\mathbf{R}$, determines the precise structure of neuronal interactions upon firing events and is indexed such that R_{kl}^{ij} denotes the recurrent connection strength between the i^{th} post-connected neuron in the k^{th} population and the j^{th} pre-connected neuron in the l^{th} population. The recurrent connectivity is prescribed by a Bernoulli distribution such that $R_{kl}^{ij} = R_{kl}/\sqrt{K}$ with probability K/N_l and $R_{kl}^{ij} = 0$ otherwise. In this case, the excitatory connection strength $R_{kE} > 0$ and the inhibitory connection strength $R_{kI} < 0$.

In addition to recurrent inputs, each population also receives upstream external inputs prescribed by constant vector $\mathbf{p_k}$, where p_k^j denotes the j^{th} component of the vector of upstream inputs driving the k^{th} downstream neuronal population. The $N \times m$ feed-forward connectivity matrix, $\mathbf{F}$, determines the connections between the upstream and downstream layers, such that F_k^{ij} denotes the feed-forward connection strength between the j^{th} component of $\mathbf{p_k}$ and the i^{th} neuron in the k^{th} population. Requiring that irregular firing activity is the result of the recurrent interactions among neurons in the downstream network, we assume the external input is constant and relatively strong, such that the expected upstream input into a neuron in the k^{th} population is $\sqrt{K} f_k m_0$, with $\mathcal{O}(1)$ parameters m_0 and f_k scaling the overall and relative external drive strengths for the two populations, respectively.

Assuming sparse connectivity, where $1 \ll K \ll N_E, N_I$, each neuron receives on average K excitatory incoming connections and K inhibitory incoming connections. Therefore, if R_{kl} is $\mathcal{O}(1)$, then only $\mathcal{O}(\sqrt{K})$ excitatory inputs are necessary for a neuron to fire given an $\mathcal{O}(1)$ threshold potential. For such recurrent connectivity, the mean excitatory and inhibitory inputs into each neuron are in total of the same order as the threshold potential, making intermittent fluctuations in input typically responsible for action potentials and their irregular distribution. As the two input types dynamically cancel over time, a nearly constant level of asynchronous neuronal activity is generally produced across the network, thereby demonstrating balanced network dynamics (van Vreeswijk and Sompolinsky 1996; Barranca et al. 2019b).

Coinciding with the irregularity of neuronal firing events as well as the dynamic balance of large excitatory and inhibitory inputs observed in response to diverse stimuli in experimental settings (Britten et al. 1993; London et al. 2010; Xue et al. 2014; Haider et al. 2006; Miura et al. 2007), we reconstruct the recurrent network connectivity given balanced network dynamics in this work. We note, however, that even if the network parameters are not strictly in the balanced operating regime, as long as the evoked dynamics are sufficiently irregular, the subsequent derivation of the input-output mapping we utilize in our reconstruction still holds, making our framework robust to alternative

network settings.

2.2 Balanced Dynamical Regime and Network Input-Output Mapping

A natural requirement for balanced dynamics is that the network activity remains non-quiescent and asynchronous in each population in the large network limit. Hence, we require the network-averaged firing rates, m_k, for $k = E, I$, to obey $0 < m_k < \infty$ as $N \to \infty$ and as $K \to \infty$ for fixed ratio N_E/N_I. Under the assumption of irregular and finite firing activity, in this section we derive a static and linear input-output relationship crucial to our framework for reconstructing network data in Section 3. In order to approximately hold for a finite network realization, the linear input-output mapping and associated theoretical bounds on the model parameters require that the network is sufficiently large and composed of enough excitatory and inhibitory connections to maintain asynchronous activity, and since this is generally the case in experimental settings of interest, the assumptions made are widely applicable. As discussed in detail in the Appendix, compressive sensing reconstruction techniques generally require *linear* measurements of *static* sampled data (Candes et al. 2006; Donoho 2006), but the system we consider here demonstrates nonlinear dynamics in time. The derived linear mapping therefore allows us to address this conceptual obstacle, and combined with limited observations of the network dynamics, we are able to efficiently reconstruct sparse network information via our extension to the CS theoretical framework.

To derive the underlying network mapping, we consider the expected voltage for each neuron in the long-time limit. To do so, we must first approximate the net effect of all recurrent and feed-forward inputs. In considering the recurrent interactions, it is important to note that the input into a particular neuron is a spike train summed over the action potentials from a relatively large number of neighboring neurons. Since the firing events of neurons in the balanced regime are weakly correlated, the summed spike train input over a large number of incoming neuronal impulses asymptotically approaches a Poisson point process (Cinlar 1972). Moreover, because the external input is constant, we arrive at an analytically tractable statistical characterization of the neuronal inputs.

Since the voltage of each neuron in the k^{th} population is reset to V_k^{Re} upon firing, we consider Eq. (1) with initial condition $v_k^i(0) = V_k^{Re}$ for $k = E, I$ in enforcing asynchronous neuronal dynamics. Assuming Poisson spike train inputs, the solution to the corresponding initial value problem gives the subthreshold membrane potential trajectory for the i^{th} neuron in the k^{th} population and may be expressed as

$$v_k^i(t) = V_k^{Re} + \sum_{\substack{j=1 \\ j\neq i}}^{N_E} R_{kE}^{ij} T_E^j(t) + \sum_{\substack{j=1 \\ j\neq i}}^{N_I} R_{kI}^{ij} T_I^j(t) + \left(\frac{1-e^{-g_L t}}{g_L}\right) \sum_j F_k^{ij} p_k^j \tag{2a}$$

$$T_l^j(t) = \sum_{s=1}^{M_l^j(t)} e^{-g_L\left(t - U_{l,s}^j(t)\right)}, \tag{2b}$$

where $R_{kl}^{ij} \cdot T_l^j(t)$ yields the total recurrent spike train input from the j^{th} neuron in the l^{th} population into the i^{th} neuron in the k^{th} population at time t and $M_l^j(t)$ denotes the corresponding total number of spikes emitted by the j^{th} neuron in the l^{th} population through time t. Note that here $M_l^j(t)$ is described approximately by a Poisson distribution with the average number of events $m_l^j t$, where m_l^j is the firing rate of the j^{th} neuron in the l^{th} population.

Corresponding to $M_l^j(t)$, the spike train input from the j^{th} neuron in the l^{th} population has spike times denoted by $U_{l,s}^j(t)$, for $s = 1, 2, \ldots$, which we assume are uniformly distributed in the interval $[0, t]$ based on the irregularity of firing events. Hence, $Y_{l,s}^j(t) = e^{-g_L(t - U_{l,s}^j(t))}$ is a random variable that takes on values in the interval $[e^{-g_L t}, 1]$. Given the probability density function for random variable $U_{l,s}^j(t)$ is $P_{U_{l,s}^j(t)}(u) = 1/t$, it follows that random variable $Y_{l,s}^j(t)$ has probability density function $P_{Y_{l,s}^j(t)}(y) = 1/(g_L t y)$ for $y \in [e^{-g_L t}, 1]$ and expected value $(1 - e^{-g_L t})/(g_L t)$.

Since $T_l^j(t)$ is given by a sum of approximately independent identically distributed random variables, it has expected value $E(T_l^j(t)) = \frac{1-e^{-g_L t}}{g_L t} m_l^j t$ for a given time horizon. Temporarily disregarding the impact of the instantaneous reset condition, the expected voltage of the i^{th} neuron in the k^{th} population at time t is thus approximately

$$\tilde{v}_k^i(t) = V_k^{Re} + \frac{1-e^{-g_L t}}{g_L} \cdot \Big(\sum_j F_k^{ij} p_k^j + \sum_{\substack{j=1 \\ j\neq i}}^{N_E} R_{kE}^{ij} m_E^j + \sum_{\substack{j=1 \\ j\neq i}}^{N_I} R_{kI}^{ij} m_I^j \Big). \tag{3}$$

In the long-time limit, $t \to \infty$, this reduces to

$$\tilde{v}_k^i = V_k^{Re} + \frac{1}{g_L}\left(\sum_j F_k^{ij} p_k^j + \sum_{\substack{j=1 \\ j\neq i}}^{N_E} R_{kE}^{ij} m_E^j + \sum_{\substack{j=1 \\ j\neq i}}^{N_I} R_{kI}^{ij} m_I^j \right) \tag{4}$$

The true expected voltage, $\bar{v}_k^i(t)$, will be lower than $\tilde{v}_k^i(t)$ since upon reaching threshold V_k^T, the voltage is instantaneously reset down to V_k^{Re}. As a result of this nonlinearity in the dynamics, since the change in voltage due to an action potential is $-(V_k^T - V_k^{Re})$ occurring with rate m_k^i, it follows that the true long-time expected voltage for the i^{th} neuron in the k^{th} population, $\bar{v}_k^i$, is approximately

$$\bar{v}_k^i = V_k^{Re} + \frac{1}{g_L}\Bigg(\sum_j F_k^{ij} p_k^j + \sum_{\substack{j=1\\ j\neq i}}^{N_E} R_{kE}^{ij} m_E^j + \sum_{\substack{j=1\\ j\neq i}}^{N_I} R_{kI}^{ij} m_I^j - m_k^i (V_k^T - V_k^{Re})\Bigg). \tag{5}$$

Eq. (5) yields a linear input-output mapping, which we will use to derive conditions on the parameters producing balanced dynamics and subsequently reconstruct network data. This key mapping may be expressed compactly across the network in matrix form as

$$\bar{\mathbf{v}} = \mathbf{V^{Re}} + \frac{1}{g_L}\left(\mathbf{Fp} + \mathbf{Rm} - \mathbf{m}\left(\mathbf{V^T} - \mathbf{V^{Re}}\right)\right), \tag{6}$$

where $\mathbf{R}$ is ordered such that the first N_E rows (columns) correspond to the N_E excitatory neurons and the next N_I rows (columns) correspond to the N_I inhibitory neurons, and we assume the same ordering for the remaining terms in Eq. (6) corresponding to the respective single neuron terms in Eq. (5).

Characterizing the dynamics at the network level, since each neuron in the l^{th} population is expected to fire at rate m_l and each neuron in the k^{th} population is expected to receive K incoming recurrent connections from the l^{th} population with individual connection strength $R_{kl}/\sqrt{K}$, the total recurrent input from the l^{th} population into a neuron in the k^{th} population is approximately a Poisson spike train with expected value $R_{kl} m_l \sqrt{K}$. As a result, taking the expectation of Eq. (5) over all network realizations, we obtain the average long-time and leading order offset in voltage from resting potential due to recurrent and feed-forward inputs for a neuron in the k^{th} population

$$d_k = \sqrt{K}\frac{1}{g_L}\left(f_k m_0 + R_{kE} m_E + R_{kI} m_I\right). \tag{7}$$

To achieve asynchronous and irregular dynamics in the large network limit, the neuronal membrane potential must remain finite as $K \to \infty$. Therefore, $f_k m_0 + R_{kE} m_E + R_{kI} m_I$ must be $\mathcal{O}(1/\sqrt{K})$ and thus vanish as $K \to \infty$ (van Vreeswijk and Sompolinsky 1998). Solving the resultant system of linear equations, we obtain

$$m_E = \frac{|R_{II}| f_E - |R_{EI}| f_I}{R_{IE}|R_{EI}| - R_{EE}|R_{II}|} m_0 \tag{8a}$$

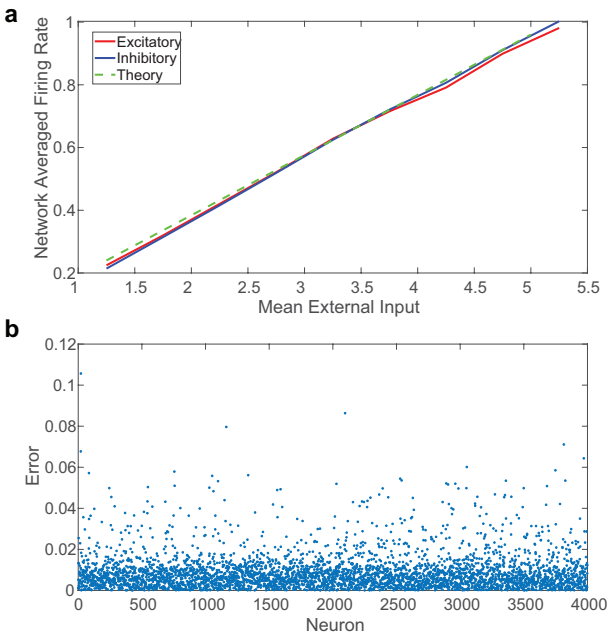


Fig. 1 Linear Input-Output Mapping. (a) Network gain curves depicting the firing rate averaged across the network as a function of the mean external input strength. The excitatory population is plotted in red, the inhibitory population is plotted in blue, and the theoretical firing rate from Eq. 8 is plotted in dashed green. (b) Absolute error in voltage computed using the derived input-output mapping (5) compared with true voltages determined via simulation. The injected current vector $\mathbf{p}$ is composed of independent and identically uniformly distributed random $\mathcal{O}(\sqrt{K})$ constant excitatory currents with population scaling such that $f_E > f_I$. In each case, a network of 2000 excitatory and 2000 inhibitory neurons is considered. Unless otherwise specified, parameters utilized are $R_{EE} = R_{IE} = 1, R_{II} = -1.8, R_{EI} = -2, f_E = 1.25, f_I = 1$, and $K = 0.0625 N_E$ in accordance with classical estimates (van Vreeswijk and Sompolinsky 1996) and the wide-spread sparsity of recurrent connectivity (He et al. 2007; Achard and Bullmore 2007; Ganmor et al. 2011; Markram et al. 1997).

$$m_I = \frac{R_{IE} f_E - R_{EE} f_I}{R_{IE}|R_{EI}| - R_{EE}|R_{II}|} m_0, \tag{8b}$$

yielding a linear scaling of the population-averaged firing rate responses with the external input strength parameter m_0.

Requiring that both the excitatory and inhibitory population-averaged firing rates are nonnegative and finite, we obtain parameter bounds

$$\frac{f_E}{f_I} > \frac{|R_{EI}|}{|R_{II}|} > \frac{R_{EE}}{R_{IE}}, \tag{9}$$

which are theoretically necessary for balanced dynamics in the large-network limit. We note that if $m_E = 0$, then solution $m_I = f_I m_0/|R_{II}|$ satisfies the linear system (8); however, in order to accurately reconstruct complete network data using the derived mapping, it

is desirable that the entire network produces irregular firing events and thus we analyze balanced dynamics in the parameter regime obeying Eq. (9).

The linear scaling of neuronal firing rates with external input strength holds both on the network level as well as for individual neurons. In Fig. 1a, we empirically examine the firing rate response of the network to increasingly large random external inputs, adjusting the external input by increasing the overall scaling strength m_0. We observe that as the mean external drive is increased, the network-averaged firing rate of both the excitatory and inhibitory populations linearly intensifies, thereby demonstrating linear gain for a finite network realization as expected theoretically in the large network limit.

On a neuron-by-neuron basis, linear mapping (5) furnishes an accurate approximation of the individual time-averaged neuronal voltages provided measurement of the neuronal firing rates and injected input currents determining the right-hand side of Eq. (5). The absolute error in the time-averaged voltages estimated using the network mapping compared to the true voltages recorded via simulation is shown in Fig. 1b across the network. For each neuron, the error is generally clustered near 0.01 and never rises above 0.12, demonstrating the high level of accuracy with which mapping (5) encodes network data and thus minor contribution of the approximations made in its derivation to the subsequent reconstructions discussed in the next section.

3 Results

3.1 Reconstruction of Recurrent Connectivity

We reconstruct the recurrent network connectivity by injecting constant currents into the network in the form of r random input vectors, denoted by $\{\mathbf{p^{(i)}}\}_{i=1}^{r}$, and record the evoked firing rates and time-averaged voltages, denoted by $\{\mathbf{m^{(i)}}\}_{i=1}^{r}$ and $\{\bar{\mathbf{v}}^{\mathbf{(i)}}\}_{i=1}^{r}$, respectively, over a short-time duration. In this case, the N^2 entries of $\mathbf{R}$ are to be reconstructed using only r trials, leading to a highly underdetermined inverse problem for $r \ll N^2$. However, since $\mathbf{R}$ is sparse, we demonstrate that compressive sensing techniques nevertheless yield an accurate reconstruction provided the appropriate network input-output mapping. A schematic of the recovery process is given in Fig. 2a.

It is important to remark that the injected current vector $\mathbf{p}$ is composed of independent and identically distributed random $\mathcal{O}(\sqrt{K})$ constant excitatory currents with population scaling such that $f_E > f_I$. Although these external inputs are not homogeneous and therefore do not strictly obey Eq. (9), asynchronous and irregular dynamics are statistically well-maintained since the random inputs have greater expected strength in the excitatory population, satisfying Eq. (9) on average for a particular realization of the injected current vector and likewise across the ensemble of input currents. Due to the finite network size in simulations, even when using homogeneous inputs, a certain subset of the neurons may exhibit unbalanced dynamics for a given realization of the external drive. However, across sufficiently many random network inputs, there are typically enough trials for which each neuron demonstrates irregular dynamics to ultimately facilitate an accurate reconstruction of recurrent network connectivity information.

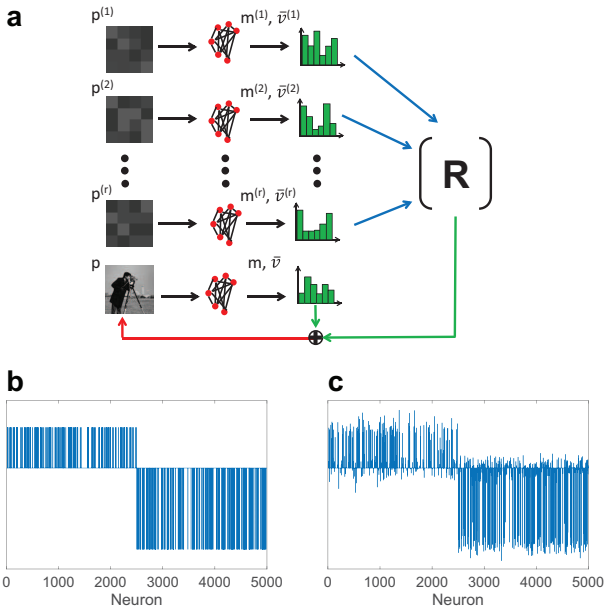


Fig. 2 Reconstruction of Recurrent Connectivity. (a) Schematic of the framework for reconstructing recurrent network connectivity and input data. The network is driven with an ensemble of r inputs, $\mathbf{p^{(1)}}, \ldots, \mathbf{p^{(r)}}$, where the evoked firing rates, $\mathbf{m^{(1)}}, \ldots, \mathbf{m^{(r)}}$, and corresponding time-averaged voltages, $\bar{\mathbf{v}}^{\mathbf{(1)}}, \ldots, \bar{\mathbf{v}}^{\mathbf{(r)}}$, are measured in each case. The derived input-output mapping (5) and recorded data are utilized to reconstruct the recurrent network connectivity matrix, $\mathbf{R}$ (indicated by blue arrows). Novel network inputs, akin to stimuli with detailed structure, $\mathbf{p}$, can then be recovered (indicated by a red arrow) by measuring the corresponding evoked neuronal firing rates and time-averaged voltages, further utilizing mapping (5) and the reconstructed recurrent connectivity matrix. (b) Sample row of the recurrent connectivity matrix for a network of 2500 excitatory and 2500 inhibitory neurons. (c) Reconstruction of the corresponding row of the recurrent connectivity matrix using 3000 inputs and recording the neuronal dynamics for 2000ms. The corresponding relative reconstruction error is 0.25 and is reduced to 0.1 if connections are thresholded.

For each injected current, linear system (5) provides an input-output map connecting the evoked network dynamics to the network input and connectivity structure. First, we consider reconstructing the recurrent connectivity matrix $\mathbf{R}$, doing so on a row-by-row basis. To recover the i^{th} row of $\mathbf{R}$, denoted $\mathbf{R}_{i*}$, we utilize the full set of inputs, $\mathbf{P} = \left[\mathbf{p^{(1)}} \dots \mathbf{p^{(r)}}\right]$, the respective firing rates of the j^{th} neuron, $\mathbf{M_j} = \left[m_j^{(1)} \dots m_j^{(r)}\right]$, for $j = 1, \dots, N$, and the respective time-averaged voltages of the i^{th} neuron only, $\mathbf{V}_i = \left[\bar{v}_i^{(1)} \dots \bar{v}_i^{(r)}\right]$.

Aggregating the i^{th} equation of input-output mapping (5) across all network inputs yields an $r \times N$ linear system in unknown recurrent connectivity matrix row $\mathbf{R}_{i*}$, having form

$$\mathbf{R}_{i*}\mathbf{M} = g_L\left(\mathbf{V_i} - (\mathbf{V^{Re}})_i\right) + \mathbf{M_i}(\mathbf{V^T} - \mathbf{V^{Re}})_i - (\mathbf{FP})_{i*}, \tag{10}$$

where matrix $\mathbf{M}$ contains the neuronal firing rates across the network for each external input realization (i.e., vector $\mathbf{M_j}$ is row j of matrix $\mathbf{M}$). Here matrix $\mathbf{M}$ is analogous to the sampling matrix in the classical CS theory framework described in the Appendix, and since the evoked network firing rate dynamics are very weakly correlated in the balanced regime, $\mathbf{M}$ is sufficiently unstructured such that it is amenable to compressive sensing sampling. Moreover, since the recurrent connectivity matrix $\mathbf{R}$ and its individual rows are sparse, the solution to Eq. (10) with minimal ℓ_1 norm yields a high fidelity reconstruction in accordance with CS theory. Solving all such linear systems for $i = 1, \dots, N$ ultimately yields the reconstruction of the full recurrent connectivity matrix.

We apply our reconstruction framework to a sample row of the recurrent connectivity matrix in Fig. 2b-C, depicting the original row and its reconstruction, respectively. From visual inspection, we see that the existence of the majority of connections, both excitatory and inhibitory, and their magnitudes are well captured, with errors primarily manifesting from the misidentification of small connections. Such extraneous connections, however, could be removed by thresholding the connection strengths in the reconstruction. To provide a quantitative measure of the reconstruction accuracy, we use the relative reconstruction error, $\|\mathbf{R} - \mathbf{R}^{\text{recon}}\|/\|\mathbf{R}\|$, and the Frobenius norm for concreteness. For a network of 5000 neurons, utilizing only 2000ms of recordings for 3000 random inputs, the reconstructed row $\mathbf{R}^{\text{recon}}$ produces a relative error of 0.25. If instead the reconstructed connections were thresholded such that sufficiently small connections were designated as errors and removed, a yet higher fidelity reconstruction is obtained in general, with a relative error of 0.1 in the case of our sample row. We remark that there is no specific enforcement of Dale's Law or a priori knowledge of the connection types in the optimization algorithm applied, and nonetheless our reconstruction framework is largely successful in distinguishing inhibitory and excitatory connections. In strictly imposing Dale's Law, sign-constrained optimization algorithms or a priori knowledge of which neurons are inhibitory may improve performance (Mishchencko et al. 2011).

It is important to note that in recovering a single row of $\mathbf{R}$, in addition to measuring the spiking dynamics over the full network, it is necessary to record only the voltage dynamics of a single neuron corresponding to the row of interest rather than the voltage of every neuron in the network. In experiments for which it is often difficult to take intracellular voltage recordings of many neurons simultaneously (Xu et al. 2017), recovering a large number of afferent connections into a single neuron may therefore be more feasible than reconstructing the full recurrent connectivity matrix. To address this limitation and generalize our methodology to the full recurrent connectivity matrix in experimental settings, recently developed near-infrared voltage indicators in combination with optogenetic stimulation (Adam et al. 2019; Abdelfattah et al. 2019), however, potentially offer the ability to record the subtreshold dynamics of neuronal networks in response to carefully controlled stimuli. As we will demonstrate in the next section, additional inputs and observation time may further improve the reconstruction quality, with the efficiency of CS theory generally increasing for larger and more sparse networks (Barranca et al. 2016a; Candes et al. 2006).

Analyzing Eq. (5) from a different perspective similarly facilitates the recovery of the network feed-forward connectivity. To recover the i^{th} row of $\mathbf{F}$, denoted $\mathbf{F}_{i*}$, we aggregate the i^{th} equation of input-output mapping (5) across all network inputs to yield $r \times m$ linear system

$$\mathbf{F}_{i*}\mathbf{P} = g_L\left(\mathbf{V_i} - (\mathbf{V^{Re}})_i\right) + \mathbf{M_i}(\mathbf{V^T} - \mathbf{V^{Re}})_i - (\mathbf{RM})_{i*}, \tag{11}$$

with solution yielding $\mathbf{F}_{i*}$. Solving the set of all such linear systems for $i = 1, \dots, N$ yields the full feed-forward connectivity. In this case $\mathbf{P}$, the matrix of injected currents across the external input ensemble, plays the role of the sampling matrix. Since the external drive is assumed random in our analysis, the sampling matrix indeed demonstrates little correlation as necessitated by CS theory. Similarly, the sparse structure of $\mathbf{F}$ facilitates efficient recovery.

In the setting of reconstructing the recurrent network connectivity, we assumed knowledge and control of the external inputs through experimental design. The feed-forward connectivity in this particular case is prescribed by an $N \times N$ diagonal matrix $\mathbf{F}$ and is chosen such that $F_{ll} = f_k$ scales the strength of the external input into all neurons in the k^{th} population, isolating $\mathbf{R}$ as the only unknown term in Eq. (10). However, if the feed-forward and recurrent connectivity are both unknown, it is generally necessary to eliminate the influence of one of the two connectivity matrices. If, for example, the recurrent connectivity is relatively weak or known, then our methodology yields an accurate reconstruction of unknown feed-forward connectivity matrix $\mathbf{F}$ of comparable quality to the recurrent connectivity reconstruction discussed previously.

3.2 Reconstruction Efficiency

In this section, we consider the efficiency of the reconstruction framework, both in terms of the size of the input ensemble utilized and the time over which the neuronal dynamics are recorded. While we determined the reconstruction of a particular row of the recurrent connectivity matrix in Fig. 2 for ease of visual comparison, we may consider Eq. (10) for $i = 1, \ldots, N$ to reconstruct the entire matrix $\mathbf{R}$ and compute its relative reconstruction error analogously. Though determining a single row of $\mathbf{R}$ required recording all neuronal firing rates and the membrane potential of a single neuron, the only necessary addition in the data needed for reconstructing the full recurrent connectivity matrix is the membrane potential dynamics of the remaining neurons.

To determine the minimal size of the input ensemble necessary for a viable reconstruction, we plot in Fig. 3a the relative reconstruction error as the number of input vectors utilized is increased. We observe an initial rapid decrease in error with input ensemble size, which saturates once sufficiently many input vectors are utilized. We see that, in comparison to the total number of connections necessary to recover, a relatively small input ensemble produces an accurate reconstruction of $\mathbf{R}$, with further trials yielding only marginal improvements. In particular, reconstructing the entire recurrent network connectivity using $r \ll N^2$ inputs injected over a short observation time of 2s reliably produces reconstruction errors less than 0.3.

We similarly investigate the necessary observation time for reconstructing the recurrent connectivity in Fig. 3b, depicting the relative reconstruction error as a function of the amount of time over which the neuronal dynamics are recorded. We note a precipitous initial decrease in error with observation time, which levels off for sufficiently long time horizons. Analogous to the dependence on input ensemble size, an efficient observation time can be selected such that further recordings yield little improvement in reconstruction quality. The saturation in error with sufficient information regarding the network dynamics suggests that the remaining error may be a consequence of the finite network size and corresponding intrinsic error in mapping (5). We expect that for a larger network, as in experimental

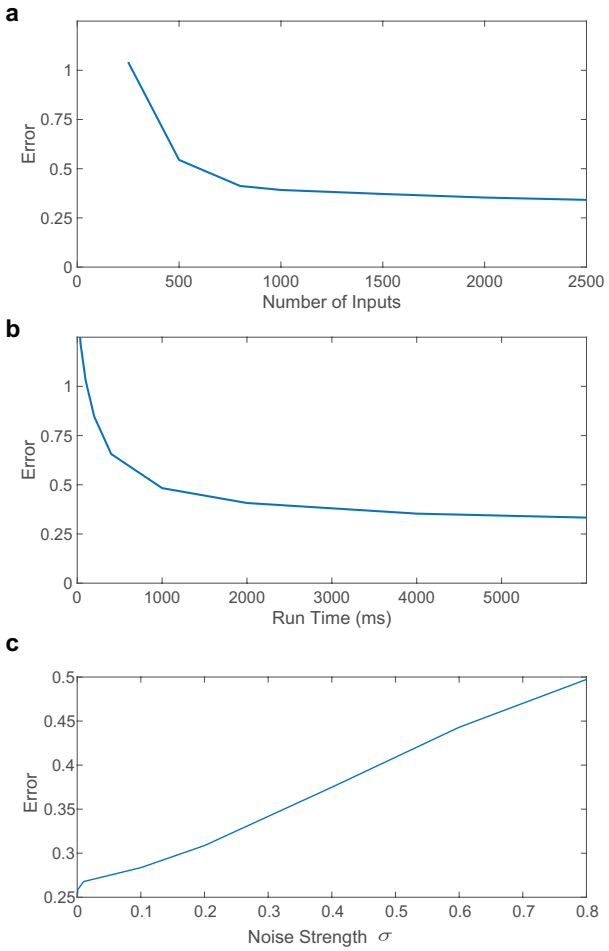


Fig. 3 Robustness of Observation Data. (a) Relative error for the reconstruction of the full recurrent connectivity matrix as a function of the number of input vectors utilized in driving the network. (b) Relative error for the reconstruction of the full recurrent connectivity matrix as a function of the duration of time over which the neuronal dynamics are measured for each injected input. The observation time utilized in (a) is 2000ms and the number of inputs utilized in (b) is 1000. In each case, the network is composed of 1000 excitatory neurons and 1000 inhibitory neurons. (c) Relative reconstruction error for the recurrent connectivity matrix row as considered in Fig. 2 with increasingly noisy measurements of the neuronal dynamics.

settings, where the neurons receive orders of magnitude more connections yet demonstrate sparser overall connectivity than investigated in this work, the dynamics will yield improved statistics and produce corresponding higher levels of efficiency in their compressive encoding of sparse network information (Candes et al. 2006; Barranca et al. 2016a).

Considering measurement error in recording neuronal dynamics is a natural source of noise present in activity data obtained experimentally (Lutcke et al. 2013; Williams and Wozny 2011), we address the impact of noise on the reconstruction quality of our framework. In recovering the row of the recurrent connectivity matrix considered in Fig. 2, we subject the voltage measurements to additive Gaussian noise with mean 0 and standard deviation σ. We observe in Fig. 3c slow growth in the relative reconstruction error with the noise standard deviation, producing reconstruction errors less than 0.3 even when σ is approximately 20% of the maximum neuronal voltage. Hence, in the presence of realistically strong noise, an accurate reconstruction is achievable.

3.3 Reconstruction of Network Inputs

Assuming the network recurrent connectivity is either known or weak, we may finally use input-output mapping (5) to recover novel network inputs with realistic structure distinct from the random input vectors utilized to reconstruct the network connectivity. To recover a network input $\mathbf{p}$ composed of m components, we utilize the evoked time-averaged neuronal voltages and firing rates measured across the network to obtain $N \times m$ linear system in unknown $\mathbf{p}$

$$\mathbf{Fp} = g_L\left(\bar{\mathbf{v}} - \mathbf{V^{Re}}\right) + \mathbf{m}\left(\mathbf{V^T} - \mathbf{V^{Re}}\right) - \mathbf{Rm}. \qquad (12)$$

For realistic sensory stimuli, $\mathbf{p}$ is typically sparse in an appropriate domain under a sparsifying transformation L such that $\hat{\mathbf{p}} = L\mathbf{p}$ (Field 1994). In the case of natural scenes, for example, a host of transformations, including the discrete versions of the Fourier, cosine, and wavelet transforms, produce a sparse representation based on the frequency domain structure of the image (Haar 1910; Heil and Walnut 1989; Donoho and Tsaig 2008). While $\mathbf{p}$ may not be sparse in its original representation, if the sparsifying transform is known, then $\mathbf{p} = L^{-1}\hat{\mathbf{p}}$ may be utilized in Eq. (12) to reconstruct sparse representation $\hat{\mathbf{p}}$ and subsequently obtain $\mathbf{p}$.

Since $\mathbf{F}$ is the sampling matrix in this case, a sufficient degree of randomness in its structure is generally required for successful recovery of input $\mathbf{p}$. While experimental measurements indicate feed-forward connectivity is often relatively structured, as in the case of receptive fields, connectivity between network layers still generally demonstrates some degree of randomness and heterogeneity (Wiesel 1960; Hubel and Wiesel 1960; Graziano and Gross 1993; Wilson 2001; Hubel 1995; Sceniak et al. 1999; Drasdo et al. 2007; Bassett and Bullmore 2006; Humphries et al. 2006). Previous theoretical analysis demonstrates that sampling matrices exhibiting a mix of localized structure and randomness in fact improve upon CS signal recovery relative to uniformly random sampling for natural stimuli (Barranca et al. 2016a; Barranca and Zhu 2018), and thus realistic feed-forward connectivity likely provides a feasible compressive sampling scheme.

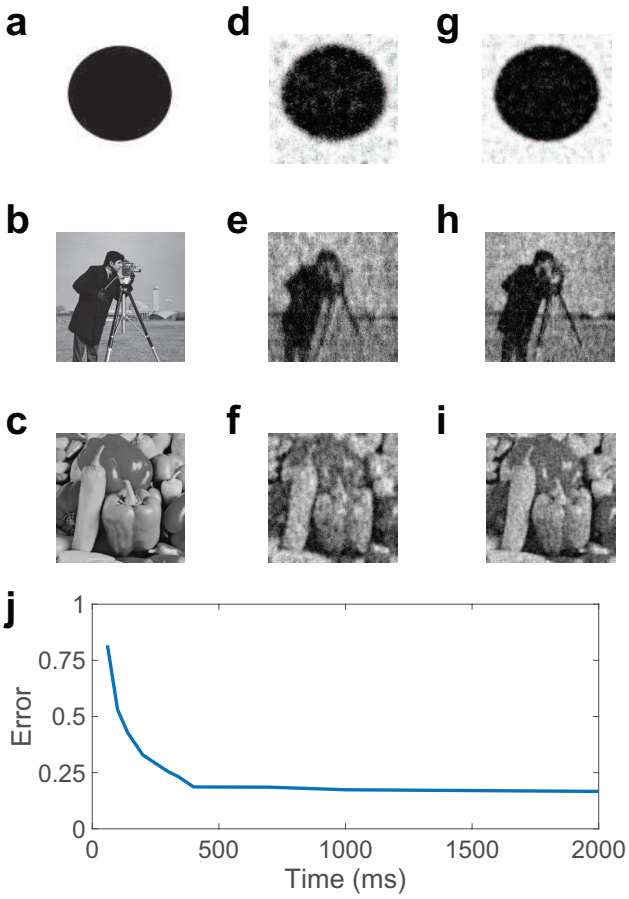


Fig. 4 Reconstruction of Network Inputs. (a)-(c) Injected images. Image (a) is composed of 100×100 pixels, image (b) is composed of 200×200 pixels, and image (c) is composed of 250×250 pixels. (d)-(f) Corresponding reconstructions utilizing a factor of 10 less neurons than pixels. (g)-(i) Corresponding reconstructions utilizing a factor of 5 less neurons than pixels. The relative reconstruction errors for (d)-(f) are $0.24, 0.31$, and 0.22, respectively. The relative reconstruction errors for (g)-(i) are $0.16, 0.25$ and 0.15, respectively. (j) Relative reconstruction error for image (a) utilizing a factor of 10 less neurons than pixels as a function of the amount of time over which the neuronal dynamics are recorded.

In Fig. 4a-c, we consider three images of various complexities and numbers of pixel components to gauge the accuracy of our reconstruction framework for natural stimuli via Eq. (12). In each case, we assume the recurrent connectivity is known and the known feed-forward connectivity matrix is composed of independent identically distributed Bernoulli random variable entries of strength f_k for inputs into neurons in the k^{th} population. We depict in Fig. 4d-f the corresponding reconstructions using a factor of 10 more pixel components than downstream neurons (i.e., $m = 10N$). We similarly exhibit in Fig. 4g-i the respective reconstructions using instead a factor of 5 more pixel components in the input stimuli. Since the number of pixel components to reconstruct is significantly larger than the number of downstream neurons (i.e., $m \gg N$), each recovery problem is highly underdetermined and amenable to compressive sensing theory.

For each image, we obtain a recognizable reconstruction, which is nearly perfect in the case of the simple dot image. As the number of downstream neurons and input pixel components becomes more comparable, we observe improved reconstruction quality. Furthermore, for images with more pixel components, which generally have more sparse representations, as in the peppers image shown in Fig. 4c, we observe greater accuracy in utilizing compressive sensing theory. This suggests that the high resolution visual stimuli encountered regularly by animals in the natural world are in fact highly compressible, and we posit that the visual system has evolved to efficiently utilize the sparse representation of prototypical inputs. Images reconstructed from the dynamics of a network with the recovered recurrent connectivity $\mathbf{R}^{\text{recon}}$ rather than the true recurrent connectivity $\mathbf{R}$ are of comparable quality to those exhibited in Fig. 4, with generally no more than a 15% difference in reconstruction error. In light of this, analyzing the encoding properties of a reconstructed network may serve as a faithful surrogate to studying the functionality of the true network.

To further gauge the efficiency of the recovery framework, in Fig. 4j, we plot the relative reconstruction error for a sample input image as a function of the amount of time over which the neuronal dynamics are recorded. Just as in the case of reconstructing the recurrent network connectivity, the error ultimately saturates for sufficiently long observation time, which in this case is only approximately 500ms. The short observation time and relatively high dimensionality of the recovered inputs indicate stimulus information is effectively encoded by the network dynamics as is the network structure.

In the early layers of many sensory systems, the number of downstream neurons is significantly less than the number of upstream neurons, as reflected in our reconstructions of natural scenes (Barlow 1981; Buck 1996). For preservation of stimulus information across networks of such disparate sizes, it is therefore necessary for neuronal network connectivity and dynamics to facilitate efficient signal processing. We hypothesize that the sparsity of natural stimuli has resulted in the selection of a strongly compressive and linear encoding of sensory information. Similarly, the complex network structure commonly found in neuronal connectivity may further facilitate efficient stimulus encoding by using a minimal number of neuronal connections and consequently little energetic resources while rapidly and accurately processing information (Humphries et al. 2006; van den Heuvel et al. 2008; Sporns and Honey 2006; Roxin et al. 2004; Barranca et al. 2019a).

4 Discussion

In the present work, we developed a novel methodology for reconstructing the recurrent connectivity of model neuronal networks using limited measurements of neuronal dynamics in response to an ensemble of random stimuli. The efficiency of our framework was crucially based on the widespread sparsity of neuronal network connectivity, utilizing compressive sensing techniques in conjunction with an embedded linear input-output relationship that we had derived in linking the recorded neuronal firing rates and voltages to the network inputs. Beyond the recurrent network connectivity, the sparsity of both natural stimuli and feed-forward connectivity furnished their efficient reconstruction using analogous techniques.

The specific form of the linear mapping we had derived was based on the irregularity of the neuronal dynamics in the balanced dynamical regime. If instead the network were composed of excitatory neurons in the mean-driven dynamical regime, the expected time-averaged voltage would be $(V_E^{Re} + V_E^T)/2$ across the network (Barranca et al. 2016b), which is precisely the mean of the firing threshold and resting membrane potentials. Therefore, when reverse-engineering network connectivity in the mean-driven case, it is only necessary to record neuronal firing events and not detailed voltage dynamics. The limitation, however, is that the strong feed-forward input generally drowns out the recurrent interactions and consequently makes it feasible to reconstruct feed-forward connectivity but highly difficult to reconstruct the recurrent network connectivity.

While we have also verified that our derived mapping holds for alternative choices of recurrent connection strength that produce irregular dynamics, determining an appropriate embedded input-output relation-

ship for alternative dynamical regimes would mark an interesting area for future investigation. In the case of synchronous dynamics, we observe a marked decrease in reconstruction accuracy and such a setting would require an alternative theoretical framework. Prior work demonstrates that the balanced state yields particularly accurate connectivity reconstructions, but even when the network dynamics are not strictly balanced theoretically, accurate recovery of recurrent connections is still achievable when the resultant dynamics are asynchronous (Barranca and Zhou 2019). We particularly focused on tight and globally balanced dynamics (Hennequin et al. 2017), but since a main theoretical requirement of the developed framework stemming from CS theory is for the neuronal activity to be irregular and primarily uncorrelated, we anticipate alternative types of balanced dynamics are amenable. Similarly, though we assumed no detailed topological structure in the recurrent network connectivity, experimental studies indicate that many brain networks demonstrate small-world, scale-free, or rich-club structure (Humphries et al. 2006; Massimini et al. 2005; Barranca et al. 2015b; Markov et al. 2013; Barranca et al. 2015a) and their connectivity reconstructions are yet to be analogously addressed.

For additional experimental suitability, it may also be possible to reconstruct neuronal connectivity using a similar methodology by injecting external input into only a subset of neurons in a larger network and then measuring the response of randomly chosen groups of neurons across trials. In most experimental settings, unobserved neurons inject hidden inputs into the recorded neurons and may potentially result in additional error in the structural connectivity inferred by our methodology (Pillow et al. 2008; Baker et al. 2020), but new theoretical approaches, such as those used to estimate the impact of hidden inputs via maximum likelihoods (Ladenbauer et al. 2019), may provide a means of accounting for the influence of shared connections from unobserved neurons. The impact of such hidden neurons in combination with potentially strong top-down inputs, such as those modulating neuronal dynamics in LGN and V1 (Angelucci and Sainsbury 2006; Sherman and Guillery 1996), may be viewed together as an additional source of the noise reflected in Fig. 3c, which if sufficiently strong could confound reconstructions.

For analytical and computational tractability, we considered the reconstruction of network data specifically in the context of a pulse-coupled integrate-and-fire neuronal network model, whose linear response properties have been well documented in the asynchronous dynamical regime and leveraged in approximating firing rate statistics as well as characterizing network encoding properties (Lindner et al. 2005; Doiron et al. 2004; Shea-Brown et al. 2008). In generalizing our framework, it is important to emphasize that alternative, more detailed, neuron models, such as the Exponential Integrate-And-Fire and Hodgkin-Huxley models, also exhibit linear gain in their firing rates in many dynamical regimes (Brunel and Latham 2003; Ostojic et al. 2009; Richardson 2004; Barranca et al. 2014a). This is also true for recurrently coupled excitatory-inhibitory spiking networks with conductance-based synapses and heterogeneous thresholds and has been applied in studying the covariation of pairwise correlations with firing rate (Barreiro and Ly 2017). We therefore anticipate that alternative choices of single neuron models and synaptic coupling, such as those reflected by alpha functions with various rise and decay timescales (Somers et al. 1995; Cai et al. 2006), are amenable to our framework upon obtaining linearized input-output curves across the network.

Similarly, neuronal firing activity measured in experiment often demonstrates a linear increase in response with external input strength (Rauch et al. 2003; La Camera et al. 2006). Thus, once an appropriate linear input-output mapping is determined through, for example, fitting a linear mapping to the individual neuronal firing rates across a small set of ramped external inputs, it is then feasible to apply our compressive sensing techniques to recover either sparse network connectivity or input stimuli. Particularly since higher dimensional signals generally demonstrate more sparsity relative to their total number of components, we expect that for realistic stimuli or network connectivity matrices with potentially billions or more entries, a sparsity-based reconstruction will provide yet larger gains in efficiency as well as accuracy.

The central role of sparsity, demonstrated by both network connectivity and stimulus structure, in our reconstruction framework underlines the importance of sparsity in the efficient coding of network information through evoked neuronal dynamics. It is possible that cortical circuits may have evolved to efficiently transmit compressed information based on this very same sparsity of natural stimuli, minimizing, for example, energy consumption while maximizing transmission speed, via complex neuronal network topologies with sparse connectivity. The precise nature in which neuronal computations interface with this sparse data remains to be investigated, but it is potentially the case that neurons intelligently utilize their sparse connectivity structure in effectively recoding information across network layers in the brain.

Appendix: Compressive Sensing Theory

Compressive sensing (CS) theory demonstrates that for signals with a sparse representation, the number of dominant components in the sparse domain determines the minimum sampling rate necessary for an accurate reconstruction. Improving upon conventional signal acquisition theory, which generally asserts that the sampling rate should instead be determined by the total number of signal components (Shannon 1949), CS theory provides an important new direction for efficient signal sampling and subsequent reconstruction (Donoho 2006; Candes et al. 2006). Considering that common signals and sensory stimuli, such as scenes, soundwaves, and odorants, as well as network connectivity are sparse in an appropriate domain (Field 1994; Markram et al. 1997; Ganmor et al. 2011; He et al. 2007), CS theory has amassed numerous and broad scientific applications (Gross et al. 2010; Lustig et al. 2007; Dai et al. 2009; Berger et al. 2010).

In developing the mathematical framework for CS theory, we consider recovering an n-component signal, $\mathbf{x}$, using a set of weighted linear measurements. Assuming m weighted measurements are utilized, the sampling scheme takes the form of an $m \times n$ sampling matrix, $\mathbf{A}$, such that each row contains a single weighted measurement. Reconstructing the signal $\mathbf{x}$ thus requires solving linear system $\mathbf{Ax} = \mathbf{b}$, where $\mathbf{b}$ is the m-vector obtained from sampling.

To reconstruct the sparsest, and thus most compressible, solution, we must select the $\mathbf{x}$ with the minimal number of non-zero components that satisfies $\mathbf{Ax} = \mathbf{b}$. Since this problem cannot be solved in polynomial time (Bruckstein et al. 2009), CS theory demonstrates that minimizing $|\mathbf{x}|_{\ell_1} = \sum_{i=1}^{n} |x_i|$ yields a reconstruction equivalent to finding the sparsest $\mathbf{x}$ for a large class of sampling matrices (Candes and Wakin 2008). The reconstruction thus requires solving

$$\arg \min_{\mathbf{x} \in R^n} |\mathbf{x}|_{\ell_1} \text{ subject to } \mathbf{Ax} = \mathbf{b}. \tag{13}$$

This specific ℓ_1 minimization problem can be efficiently solved using a host of algorithms, such as the orthogonal matching pursuit (OMP), the least angle regression (LARS), and the least absolute shrinkage and selection operator (LASSO) methods (Tropp and Gilbert 2007; Donoho and Tsaig 2008), making the reconstruction computationally feasible even for relatively large signals. Moreover, if signal $\mathbf{x}$ is not sparse in the sampled domain, but is instead sparse under a transform, L, then the linear system $\boldsymbol{\phi}\hat{\mathbf{x}} = \mathbf{b}$, where $\boldsymbol{\phi} = \mathbf{A}L^{-1}$ and $\hat{\mathbf{x}} = L\mathbf{x}$, can be considered similarly. In this particular work, OMP is applied in all reconstructions. The recovered recurrent connectivity exhibits minor variations when utilizing other standard optimization algorithms, but the optimal reconstruction accuracy is comparable in each case.

In determining an appropriate sampling scheme, it is important to note CS theory demonstrates that sampling matrices exhibiting sufficiently little correlation among their columns and approximately preserving the magnitude of sampled signals generally yield successful reconstructions of sparse signals (Candes and Wakin 2008; Baraniuk 2007). A broad class of matrices demonstrating randomness in their structure have been proven to exhibit these properties (Candes et al. 2006; Candes and Wakin 2008), and there are consequently numerous sampling schemes amenable to CS reconstruction.

Acknowledgements This work was supported by NSF grant DMS-1812478 and a Swarthmore Faculty Research Support Grant.

Conflict of interest The author declares no confict of interest.

References

L.F. Abbott. Lapicque's introduction of the integrate-and-fire model neuron (1907). *Brain research bulletin*, 50(5-6): 303–304, 1999.

A. S. Abdelfattah, T. Kawashima, A. Singh, O. Novak, H. Liu, Y. Shuai, Y. C. Huang, L. Campagnola, S. C. Seeman, J. Yu, J. Zheng, J. B. Grimm, R. Patel, J. Friedrich, B. D. Mensh, L. Paninski, J. J. Macklin, G. J. Murphy, K. Podgorski, B. J. Lin, T. W. Chen, G. C. Turner, Z. Liu, M. Koyama, K. Svoboda, M. B. Ahrens, L. D. Lavis, and E. R. Schreiter. Bright and photostable chemigenetic indicators for extended in vivo voltage imaging. *Science*, 365 (6454):699–704, 08 2019.

S. Achard and E. Bullmore. Efficiency and cost of economical brain functional networks. *PLoS Comput. Biol.*, 3(2):e17, Feb 2007.

Y. Adam, J. J. Kim, S. Lou, Y. Zhao, M. E. Xie, D. Brinks, H. Wu, M. A. Mostajo-Radji, S. Kheifets, V. Parot, S. Chettih, K. J. Williams, B. Gmeiner, S. L. Farhi, L. Madisen, E. K. Buchanan, I. Kinsella, D. Zhou, L. Paninski, C. D. Harvey, H. Zeng, P. Arlotta, R. E. Campbell, and A. E. Cohen. Voltage imaging and optogenetics reveal behaviour-dependent changes in hippocampal dynamics. *Nature*, 569(7756):413–417, 05 2019.

A. Angelucci and K. Sainsbury. Contribution of feedforward thalamic afferents and corticogeniculate feedback to the spatial summation area of macaque V1 and LGN. *J. Comp. Neurol.*, 498(3):330–351, Sep 2006.

C. Baker, E. Froudarakis, D. Yatsenko, A. S. Tolias, and R. Rosenbaum. Inference of synaptic connectivity and external variability in neural microcircuits. *J. Comput. Neurosci.*, 48(2):123–147, 05 2020.

R. Baraniuk. Compressive sensing. *IEEE Signal Processing Mag*, pages 118–120, 2007.

H B Barlow. The ferrier lecture, 1980. critical limiting factors in the design of the eye and visual cortex. *Proc R Soc Lond B Biol Sci*, 212(1186):1–34, May 1981. ISSN 0080-4649 (Print); 0080-4649 (Linking).

V. J. Barranca and D. Zhou. Compressive Sensing Inference of Neuronal Network Connectivity in Balanced Neuronal Dynamics. *Front Neurosci*, 13:1101, 2019.

V. J. Barranca and X. G. Zhu. A computational study of the role of spatial receptive field structure in processing natural and non-natural scenes. *J. Theor. Biol.*, 454:268–277, Oct 2018.

V. J. Barranca, D. C. Johnson, J. L. Moyher, J. P. Sauppe, M. S. Shkarayev, G. Kovačič, and D. Cai. Dynamics of the exponential integrate-and-fire model with slow currents and adaptation. *J. Comput. Neurosci.*, 37(1):161–180, Aug 2014a.

V. J. Barranca, G. Kovačič, D. Zhou, and D. Cai. Sparsity and compressed coding in sensory systems. *PLoS Comput. Biol.*, 10(8):e1003793, Aug 2014b.

V. J. Barranca, D. Zhou, and D. Cai. A novel characterization of amalgamated networks in natural systems. *Sci Rep*, 5: 10611, Jun 2015a.

V. J. Barranca, D. Zhou, and D. Cai. Low-rank network decomposition reveals structural characteristics of small-world networks. *Phys Rev E Stat Nonlin Soft Matter Phys*, 92(6):062822, Dec 2015b.

V. J. Barranca, G. Kovačič, D. Zhou, and D. Cai. Improved Compressive Sensing of Natural Scenes Using Localized Random Sampling. *Sci. Rep.*, 6:31976, Aug 2016a.

V. J. Barranca, H. Huang, and G. Kawakita. Network structure and input integration in competing firing rate models for decision-making. *J Comput Neurosci*, 46(2):145–168, Apr 2019a.

V. J. Barranca, H. Huang, and S. Li. The impact of spike-frequency adaptation on balanced network dynamics. *Cogn Neurodyn*, 13(1):105–120, Feb 2019b.

V.J. Barranca, D. Zhou, and D. Cai. Compressive sensing reconstruction of feed-forward connectivity in pulse-coupled nonlinear networks. *Phys. Rev. E*, 93:060201, Jun 2016b. doi: 10.1103/PhysRevE.93.060201.

A. K. Barreiro and C. Ly. When do correlations increase with firing rates in recurrent networks? *PLoS Comput. Biol.*, 13 (4):e1005506, 04 2017.

N. Barros-Zulaica, J. Rahmon, G. Chindemi, R. Perin, H. Markram, E. Muller, and S. Ramaswamy. Estimating the Readily-Releasable Vesicle Pool Size at Synaptic Connections in the Neocortex. *Front. Synaptic Neurosci.*, 11: 29, 2019.

D.S. Bassett and E. Bullmore. Small-world brain networks. *Neuroscientist*, 12(6):512–523, Dec 2006. ISSN 1073-8584 (Print); 1073-8584 (Linking). doi: 10.1177/1073858406293182.

C.R. Berger, z. Wang, J. Huang, and S. Zhou. Application of compressive sensing to sparse channel estimation. *Comm. Mag.*, 48(11), 2010.

S. Boccaletti, V. Latora, Y. Moreno, M. Chavez, and D.-U. Hwang. Complex networks: Structure and dynamics. *Phys. Rep.*, 424:175–308, 2006.

A.A. Boulton, G.B. Baker, and C.H. Vanderwolf. *Neurophysiological Techniques: Applications to Neural Systems*. Neurophysiological Techniques. Humana Press, 1990. ISBN 9781592596201.

R. Brette, M. Rudolph, T. Carnevale, M. Hines, D. Beeman, J. M. Bower, M. Diesmann, A. Morrison, P. H. Goodman, F. C. Harris Jr, M. Zirpe, T. Natschlager, D. Pecevski, B. Ermentrout, M. Djurfeldt, A. Lansner, O. Rochel, T. Vieville, E. Muller, A. P. Davison, S. El Boustani, and A. Destexhe. Simulation of networks of spiking neurons: A review of tools and strategies. *J. Comput. Neurosci.*, 23 (3):349–398, December 2007.

K. L. Briggman and D. D. Bock. Volume electron microscopy for neuronal circuit reconstruction. *Curr. Opin. Neurobiol.*, 22(1):154–161, Feb 2012.

K. H. Britten, M. N. Shadlen, W. T. Newsome, and J. A. Movshon. Responses of neurons in macaque MT to stochastic motion signals. *Vis. Neurosci.*, 10(6):1157–1169, 1993.

A.M. Bruckstein, D.L. Donoho, and M. Elad. From sparse solutions of systems of equations to sparse modeling of signals and images. *SIAM Review*, 51(1):34–81, 2009.

N. Brunel and P. Latham. Firing rate of the noisy quadratic integrate-and-fire neuron. *Neural Comp.*, 15:2281–2306, 2003.

L.B. Buck. Information coding in the vertebrate olfactory system. *Annu Rev Neurosci*, 19:517–544, 1996. ISSN 0147-006X (Print); 0147-006X (Linking). doi: 10.1146/annurev.ne.19.030196.002505.

A.N. Burkitt. A review of the integrate-and-fire neuron model: I. homogeneous synaptic input. *Biol. Cybern.*, 95(1):1–19, 2006. ISSN 0340-1200 (Print). doi: 10.1007/s00422-006-0068-6.

D. Cai, L. Tao, A. V. Rangan, and D. W. McLaughlin. Kinetic theory for neuronal network dynamics. *Commun. Math. Sci.*, 4(1):97–127, 2006.

E. J. Candes and M. B. Wakin. An Introduction To Compressive Sampling. *Signal Process. Mag., IEEE*, 25(2):21–30, March 2008. ISSN 1053-5888.

E.J. Candes, J.K. Romberg, and T. Tao. Stable signal recovery from incomplete and inaccurate measurements. *Commun. Pur. Appl. Math.*, 59(8):1207–1223, 2006. ISSN 1097-0312.

R. Cestnik and M. Rosenblum. Reconstructing networks of pulse-coupled oscillators from spike trains. *Phys. Rev. E*, 96(1-1):012209, Jul 2017.

E. Cinlar. Superposition of point processes. In P.A.W. Lewis, editor, *Stochastic Point Processes: Statistical Analysis, Theory, and Applications*, pages 549–606. Wiley, New York, NY, 1972.

R. Dahlhaus, M. Eichler, and J. Sandkuhler. Identification of synaptic connections in neural ensembles by graphical models. *J. Neurosci. Methods*, 77(1):93–107, Nov 1997.

W. Dai, M. A. Sheikh, O. Milenkovic, and R. G. Baraniuk. Compressive sensing DNA microarrays. *J. Bioinform. Syst. Biol.*, page 162824, 2009.

Ildefons Magrans de Abril, Junichiro Yoshimoto, and Kenji Doya. Connectivity inference from neural recording data: Challenges, mathematical bases and research directions. *Neural Networks*, 102:120–137, 2018.

B. Doiron, B. Lindner, A. Longtin, L. Maler, and J. Bastian. Oscillatory activity in electrosensory neurons increases with the spatial correlation of the stochastic input stimulus. *Phys. Rev. Lett.*, 93(4):048101, Jul 2004.

D.L. Donoho. Compressed sensing. *IEEE Trans. Info. Theory*, 52(4):1289–1306, 2006.

D.L. Donoho and Y. Tsaig. Fast solution of l_1-norm minimization problems when the solution may be sparse. *IEEE Trans. Inform. Theory*, 54(11):4789–4812, 2008.

N. Drasdo, C.L. Millican, C.R. Katholi, and C.A. Curcio. The length of henle fibers in the human retina and a model of ganglion receptive field density in the visual field. *Vision research*, 47(22):2901–2911, 2007.

D.J. Field. What is the goal of sensory coding? *Neural Computation*, 6(4):559–601, 2012/10/27 1994. doi: 10.1162/neco.1994.6.4.559.

G. D. Field, J. L. Gauthier, A. Sher, M. Greschner, T. A. Machado, L. H. Jepson, J. Shlens, D. E. Gunning, K. Mathieson, W. Dabrowski, L. Paninski, A. M. Litke, and E. J. Chichilnisky. Functional connectivity in the retina at the resolution of photoreceptors. *Nature*, 467(7316):673–677, Oct 2010.

K. J. Friston. Functional and effective connectivity: a review. *Brain Connect*, 1(1):13–36, 2011.

E. Ganmor, R. Segev, and E. Schneidman. The architecture of functional interaction networks in the retina. *J. Neurosci.*, 31(8):3044–3054, Feb 2011.

M. S. Graziano and C. G. Gross. A bimodal map of space: somatosensory receptive fields in the macaque putamen with corresponding visual receptive fields. *Exp Brain Res*, 97 (1):96–109, 1993.

B. F. Grewe, D. Langer, H. Kasper, B. M. Kampa, and F. Helmchen. High-speed in vivo calcium imaging reveals neuronal network activity with near-millisecond precision. *Nat. Methods*, 7(5):399–405, May 2010.

D. Gross, Y. K. Liu, S. T. Flammia, S. Becker, and J. Eisert. Quantum state tomography via compressed sensing. *Phys.*

Rev. Lett., 105(15):150401, Oct. 2010.

A. Haar. Zur Theorie der orthogonalen Funktionensysteme. *Mathematische Annalen*, 69(3):331–371, September 1910.

Patric Hagmann, Leila Cammoun, Xavier Gigandet, Reto Meuli, Christopher J Honey, Van J Wedeen, and Olaf Sporns. Mapping the structural core of human cerebral cortex. *PLoS biology*, 6(7):e159, 2008.

B. Haider, A. Duque, A. R. Hasenstaub, and D. A. McCormick. Neocortical network activity in vivo is generated through a dynamic balance of excitation and inhibition. *J. Neurosci.*, 26(17):4535–4545, Apr 2006.

Y. He, Z. J. Chen, and A. C. Evans. Small-world anatomical networks in the human brain revealed by cortical thickness from MRI. *Cereb. Cortex*, 17(10):2407–2419, Oct 2007.

C.E. Heil and D.F. Walnut. Continuous and discrete wavelet transforms. *SIAM review*, 31(4):628–666, 1989.

G. Hennequin, E. J. Agnes, and T. P. Vogels. Inhibitory Plasticity: Balance, Control, and Codependence. *Annu. Rev. Neurosci.*, 40:557–579, 07 2017.

S. Holler, G. Köstinger, K. A. C. Martin, G. F. P. Schuhknecht, and K. J. Stratford. Structure and function of a neocortical synapse. *Nature*, 591(7848):111–116, 03 2021.

Christopher J Honey, Olaf Sporns, Leila Cammoun, Xavier Gigandet, Jean-Philippe Thiran, Reto Meuli, and Patric Hagmann. Predicting human resting-state functional connectivity from structural connectivity. *Proceedings of the National Academy of Sciences*, 106(6):2035–2040, 2009.

Barry Horwitz. The elusive concept of brain connectivity. *Neuroimage*, 19(2):466–470, 2003.

D. H. Hubel and T. N. Wiesel. Receptive fields of optic nerve fibres in the spider monkey. *J Physiol*, 154:572–580, Dec 1960. ISSN 0022-3751 (Print); 0022-3751 (Linking).

D.H. Hubel. *Eye, Brain, and Vision*. Scientific American Library Series. Henry Holt and Company, New York, 1995. ISBN 9780716760092.

M.D. Humphries, K. Gurney, and T.J. Prescott. The brainstem reticular formation is a small-world, not scale-free, network. *Proc. Biol. Sci.*, 273(1585):503–511, Feb 2006. ISSN 0962-8452 (Print); 0962-8452 (Linking). doi: 10.1098/rspb.2005.3354.

X. Jiang, S. Shen, C. R. Cadwell, P. Berens, F. Sinz, A. S. Ecker, S. Patel, and A. S. Tolias. Principles of connectivity among morphologically defined cell types in adult neocortex. *Science*, 350(6264):aac9462, Nov 2015.

G. La Camera, A. Rauch, D. Thurbon, H. R. Luscher, W. Senn, and S. Fusi. Multiple time scales of temporal response in pyramidal and fast spiking cortical neurons. *J. Neurophysiol.*, 96(6):3448–3464, Dec 2006.

J. Ladenbauer, S. McKenzie, D. F. English, O. Hagens, and S. Ostojic. Inferring and validating mechanistic models of neural microcircuits based on spike-train data. *Nat. Commun.*, 10(1):4933, 10 2019.

B. Lindner, B. Doiron, and A. Longtin. Theory of oscillatory firing induced by spatially correlated noise and delayed inhibitory feedback. *Phys. Rev. E*, 72(6 Pt 1):061919, Dec 2005.

M. London, A. Roth, L. Beeren, M. Hausser, and P. E. Latham. Sensitivity to perturbations in vivo implies high noise and suggests rate coding in cortex. *Nature*, 466 (7302):123–127, Jul 2010.

M. Lustig, D. Donoho, and J. M. Pauly. Sparse MRI: The application of compressed sensing for rapid MR imaging. *Magn. Reson. Med.*, 58(6):1182–1195, Dec. 2007.

H. Lutcke, F. Gerhard, F. Zenke, W. Gerstner, and F. Helmchen. Inference of neuronal network spike dynamics and topology from calcium imaging data. *Front. Neural. Circuits*, 7:201, 2013.

N. T. Markov, M. Ercsey-Ravasz, D. C. Van Essen, K. Knoblauch, Z. Toroczkai, and H. Kennedy. Cortical high-density counterstream architectures. *Science*, 342 (6158):1238406, Nov 2013.

H. Markram, J. Lubke, M. Frotscher, A. Roth, and B. Sakmann. Physiology and anatomy of synaptic connections between thick tufted pyramidal neurones in the developing rat neocortex. *J. Physiol.*, 500 (Pt 2):409–440, Apr 1997. ISSN 0022-3751 (Print); 0022-3751 (Linking).

M. Massimini, F. Ferrarelli, R. Huber, S. K. Esser, H. Singh, and G. Tononi. Breakdown of cortical effective connectivity during sleep. *Science*, 309(5744):2228–2232, Sep 2005.

W. Mather, M. R. Bennett, J. Hasty, and L. S. Tsimring. Delay-induced degrade-and-fire oscillations in small genetic circuits. *Phys. Rev. Lett.*, 102(6):068105, Feb 2009.

D. McLaughlin, R. Shapley, M. Shelley, and J. Wielaard. A neuronal network model of macaque primary visual cortex (V1): Orientation selectivity and dynamics in the input layer $4C\alpha$. *Proc. Natl. Acad. Sci. USA*, 97:8087–8092, 2000.

Yuriy Mishchencko, Joshua T Vogelstein, and Liam Paninski. A bayesian approach for inferring neuronal connectivity from calcium fluorescent imaging data. *The Annals of Applied Statistics*, pages 1229–1261, 2011.

K. Miura, Y. Tsubo, M. Okada, and T. Fukai. Balanced excitatory and inhibitory inputs to cortical neurons decouple firing irregularity from rate modulations. *J. Neurosci.*, 27 (50):13802–13812, Dec 2007.

S. Ostojic, N. Brunel, and V. Hakim. How connectivity, background activity, and synaptic properties shape the cross-correlation between spike trains. *J. Neurosci.*, 29(33): 10234–10253, Aug 2009.

A. M. Packer, L. E. Russell, H. W. Dalgleish, and M. Hausser. Simultaneous all-optical manipulation and recording of neural circuit activity with cellular resolution in vivo. *Nat. Methods*, 12(2):140–146, Feb 2015.

Jonathan W Pillow, Jonathon Shlens, Liam Paninski, Alexander Sher, Alan M Litke, EJ Chichilnisky, and Eero P Simoncelli. Spatio-temporal correlations and visual signalling in a complete neuronal population. *Nature*, 454 (7207):995–999, 2008.

A. V. Rangan and D. Cai. Maximum-entropy closures for kinetic theories of neuronal network dynamics. *Phys. Rev. Lett.*, 96(17):178101, 2006.

A. Rauch, G. La Camera, H.R. Luscher, W. Senn, and S. Fusi. Neocortical pyramidal cells respond as integrate-and-fire neurons to in vivo-like input currents. *J Neurophysiol*, 90 (3):1598–1612, Sep 2003. ISSN 0022-3077 (Print); 0022-3077 (Linking). doi: 10.1152/jn.00293.2003.

Magnus J E Richardson. Effects of synaptic conductance on the voltage distribution and firing rate of spiking neurons. *Phys Rev E Stat Nonlin Soft Matter Phys*, 69(5 Pt 1): 051918, May 2004. ISSN 1539-3755 (Print).

J. P. Rickgauer, K. Deisseroth, and D. W. Tank. Simultaneous cellular-resolution optical perturbation and imaging of place cell firing fields. *Nat. Neurosci.*, 17(12):1816–1824, Dec 2014.

A. Roxin, H. Riecke, and S.A. Solla. Self-sustained activity in a small-world network of excitable neurons. *Phys. Rev. Lett.*, 92:198101, May 2004. doi: 10.1103/PhysRevLett.92.198101.

E. Salinas and T. J. Sejnowski. Correlated neuronal activity and the flow of neural information. *Nat. Rev. Neurosci.*, 2 (8):539–550, Aug 2001.

A. Sawatari and E.M. Callaway. Diversity and cell type specificity of local excitatory connections to neurons in layer 3B of monkey primary visual cortex. *Neuron*, 25, 2000.

M. P. Sceniak, D. L. Ringach, M. J. Hawken, and R. Shapley. Contrast's effect on spatial summation by macaque V1 neurons. *Nat. Neurosci.*, 2(8):733–739, Aug 1999.

C. E. Shannon. Communication in the Presence of Noise. *Proceedings of the IRE*, 37(1):10–21, January 1949. ISSN 0096-8390.

E. Shea-Brown, K. Josić, J. de la Rocha, and B. Doiron. Correlation and synchrony transfer in integrate-and-fire neurons: basic properties and consequences for coding. *Phys. Rev. Lett.*, 100(10):108102, Mar 2008.

S Murray Sherman and RW Guillery. Functional organization of thalamocortical relays. *Journal of neurophysiology*, 76 (3):1367–1395, 1996.

M. Shimono and J. M. Beggs. Functional Clusters, Hubs, and Communities in the Cortical Microconnectome. *Cereb. Cortex*, 25(10):3743–3757, Oct 2015.

D. Somers, S. Nelson, and M. Sur. An emergent model of orientation selectivity in cat visual cortical simple cells. *Journal of Neuroscience*, 15:5448–5465, 1995.

Sen Song, Per Jesper Sjostrom, Markus Reigl, Sacha Nelson, and Dmitri B Chklovskii. Highly nonrandom features of synaptic connectivity in local cortical circuits. *PLoS Biol.*, 3(3):e68, Mar 2005. ISSN 1545-7885 (Electronic); 1544-9173 (Linking). doi: 10.1371/journal.pbio.0030068.

O. Sporns and C.J. Honey. Small worlds inside big brains. *Proc Natl Acad Sci U S A*, 103(51):19219–19220, Dec 2006. ISSN 0027-8424 (Print); 0027-8424 (Linking). doi: 10.1073/pnas.0609523103.

O. Stetter, D. Battaglia, J. Soriano, and T. Geisel. Model-free reconstruction of excitatory neuronal connectivity from calcium imaging signals. *PLoS Comput. Biol.*, 8(8): e1002653, 2012.

I. H. Stevenson, J. M. Rebesco, L. E. Miller, and K. P. Kording. Inferring functional connections between neurons. *Curr. Opin. Neurobiol.*, 18(6):582–588, Dec 2008.

J. A. Tropp and A. C. Gilbert. Signal Recovery From Random Measurements Via Orthogonal Matching Pursuit. *IEEE Trans. Inform. Theory*, 53(12):4655–4666, December 2007. ISSN 0018-9448.

T. W. Troyer and K. D. Miller. Physiological gain leads to high ISI variability in a simple model of a cortical regular spiking cell. *Neural Comput*, 9(5):971–983, Jul 1997.

M. Tsodyks and C. Gilbert. Neural networks and perceptual learning. *Nature*, 431(7010):775–781, Oct 2004.

M.P. van den Heuvel, C.J. Stam, M. Boersma, and H.E. Hulshoff Pol. Small-world and scale-free organization of voxel-based resting-state functional connectivity in the human brain. *Neuroimage*, 43(3):528–539, Nov 2008. ISSN 1095-9572 (Electronic); 1053-8119 (Linking). doi: 10.1016/j.neuroimage.2008.08.010.

C. van Vreeswijk and H. Sompolinsky. Chaos in neuronal networks with balanced excitatory and inhibitory activity. *Science*, 274:1724–1726, 1996.

C. van Vreeswijk and H. Sompolinsky. Chaotic balanced state in a model of cortical circuits. *Neural Comput.*, 15:1321–1371, 1998.

R. Vicente, M. Wibral, M. Lindner, and G. Pipa. Transfer entropy–a model-free measure of effective connectivity for the neurosciences. *J. Comput. Neurosci.*, 30(1):45–67, Feb 2011.

N. R. Wall, I. R. Wickersham, A. Cetin, M. De La Parra, and E. M. Callaway. Monosynaptic circuit tracing in vivo through Cre-dependent targeting and complementation of modified rabies virus. *Proc. Natl. Acad. Sci. U.S.A.*, 107 (50):21848–21853, Dec 2010.

T. N. Wiesel. Receptive fields of ganglion cells in the cat's retina. *J Physiol*, 153:583–594, Oct 1960. ISSN 0022-3751 (Print); 0022-3751 (Linking).

S. R. Williams and C. Wozny. Errors in the measurement of voltage-activated ion channels in cell-attached patch-clamp recordings. *Nat. Commun.*, 2:242, 2011.

D. A. Wilson. Receptive fields in the rat piriform cortex. *Chem. Senses*, 26(5):577–584, Jun 2001.

Y. Xu, P. Zou, and A. E. Cohen. Voltage imaging with genetically encoded indicators. *Curr. Opin. Chem. Biol.*, 39: 1–10, Aug 2017.

M. Xue, B. V. Atallah, and M. Scanziani. Equalizing excitation-inhibition ratios across visual cortical neurons. *Nature*, 511(7511):596–600, Jul 2014.

Y. V. Zaytsev, A. Morrison, and M. Deger. Reconstruction of recurrent synaptic connectivity of thousands of neurons from simulated spiking activity. *J. Comput. Neurosci.*, 39 (1):77–103, Aug 2015.

D. Zhou, Y. Xiao, Y. Zhang, Z. Xu, and D. Cai. Causal and structural connectivity of pulse-coupled nonlinear networks. *Phys. Rev. Lett.*, 111(5):054102, Aug 2013.